



Assessment of Fluid Forces on Flooded Bridge Superstructures Using the SPH Method

T. A. Do¹ , T. H. Nguyen^{1*} 

¹ Faculty of Civil Engineering, University of Transport and Communications, Hanoi, Vietnam.

Received 30 August 2024; Revised 13 November 2024; Accepted 21 November 2024; Published 01 December 2024

Abstract

This paper presents a numerical simulation utilizing the Smoothed Particle Hydrodynamics (SPH) methodology to analyze the impact of water flow on bridge superstructures. The focus of the study is the Canh Nang bridge, which experienced significant damage during a severe flood in Vietnam. The SPH model accounts for flow morphology, velocity fields, and flow pressure around the submerged superstructure, providing insights into areas of high flow pressure and the water resistance coefficient (Cd). By employing modified dynamic boundaries for solid surfaces and the inflow-outflow conditions, the model effectively addresses fluid-bed and fluid-structure interactions. The results highlight elevated flow pressure on specific surface locations of the superstructure, while lower pressures are observed on the bottom surfaces and between adjacent girders. The calculated Cd values are evaluated against those from various bridge design standards, including the Indian code, Eurocode, AS5100, and TCVN 11823. This comparison reveals discrepancies and suggests the potential for refining current design practices. Future research directions include the experimental validation of SPH model results and the exploration of how structural parameters influence superstructure response during flood events.

Keywords: SPH; Bridge Superstructure; Flow-Structure Interaction; Flow Impact Force; Canh Nang Bridge.

1. Introduction

In recent years, many bridges have been collapsed or damaged due to floods and natural disasters. For instance, the Hatchie Bridge [1] in Tennessee was damaged in April 1989, the Schoharie Creek Bridge [2] in New York was damaged in 1987, and the Hintze Ribeiro Bridge [3] in Portugal was damaged in 2001. In Indonesia, the powerful earthquake and tsunami of December 2004 led to the failure of multiple bridges [4]. The instability of the piers might have contributed to the damage to these bridges.

Most recently, in 2011, the tsunamis triggered by the Great East Japan Earthquake destroyed 300 bridges, leading to serious disruptions in the national lifeline system [5]. This not only delayed rescue operations but also impeded the recovery efforts for the affected towns and cities. Therefore, exploring ways to strengthen bridges in tsunami-prone coastal areas is compulsory. Most efforts have been focused on determining whether bridge bearings and/or connecting cables possess the necessary strength to prevent structures from being washed away by waves. Additionally, fluid dynamic-related countermeasures have proven valuable in bridge engineering, particularly in wind engineering. By applying dynamic fluid engineering techniques, it is possible to identify optimized cross-sectional designs that can minimize hydrodynamic forces on bridges.

To solve the problem of fluid-structure interaction, Hirt & Nichols [6] and Xiao et al. [7] used the Volume of Fluid (VOF) scheme to evaluate wave-current forces on horizontal cylinders with free surfaces. Nan et al. [8] employed a

* Corresponding author: nhthuan@utc.edu.vn

 <http://dx.doi.org/10.28991/CEJ-2024-010-12-019>



© 2024 by the authors. Licensee C.E.J, Tehran, Iran. This article is an open access article distributed under the terms and conditions of the Creative Commons Attribution (CC-BY) license (<http://creativecommons.org/licenses/by/4.0/>).

coupled Volume of Fluid-Fluid Structure Interaction (VOF-FSI) to identify significant changes in the vortex around bridges. The stress-strain and deformation results obtained from the numerical simulations corresponded with the observed breakage locations at the site. Another study by Song et al. [9], also based on the VOF method, investigated the impact of waves on girder bridge decks and calculated the lateral and lift forces from the flow while accounting for the influence of upstream and downstream water depths. However, the VOF-based method has limitations in tracking free surfaces and the interaction interface between the flow and the solid surface. Furthermore, these models did not fully compute or analyze the fluid pressures at various points on the structural surfaces.

Several recent studies have also used different methods to simulate the interaction between flow and structures. Among these, Tang et al. [10] developed a numerical model to study the impact of waves on bridge decks near sloping seabeds using OpenFOAM (based on the CFD method). This model analyzed the effects of wave characteristics, submersion coefficients, and slope inclinations on wave forces. The results showed that wave forces on the bridge are influenced by the interactions between incoming and reflected waves, the bridge's position relative to the sloping seabed, and the slope angle. The findings highlight the complicated dynamic influence of wave forces on the bridge and underscore the significance of accounting for seabed topography when designing a bridge. Han et al. [11] and Wang et al. [12] established safety assessment models for box-girder bridge structures under wave impacts. The Tsunami Squares (TS) and CFD meshless methods were used to predict wave motion and calculate the maximum horizontal and vertical wave loads on box girders. In a study by Kisi et al. [13], the authors calculated the mean upstream and downstream flow velocities using four data-driven methods consisting of multilinear regression (MLR), M5Tree, Gaussian process regression, and multivariate adaptive regression spline. Overall, numerical simulations in these studies were limited in their ability to compute the fluid pressure field on structural surfaces or to capture real-time flow morphology when interacting with bridge structures.

Within the domain of experimental study of the interaction of structures and fluid, several research studies have been done to assess the fluid forces acting on bridges. Kosa et al. [14] carried out an experiment to assess the horizontal force on bridges caused by tsunamis. Liang et al. [15] conducted experiments associated with the breaking tsunami wave loading on a bridge deck. Liang et al. [15] performed experiments on the force of tsunamis acting on bridge models. Zhang et al. [16] conducted experimental research on countermeasures aimed at reducing tsunami wave forces on bridge superstructures.

To address the fluid-structure interaction between water flow and bridges, the SPH method can be employed. This numerical technique is well suited for computing flow with free surfaces. The SPH method, initially presented by G. Gingold & Monaghan [17] and Lucy [18] for problems of astrophysics, has been recently used in other fields such as the impact of solids [19-27]. Additionally, the SPH modeling has been adapted to tackle the dynamic responses of largely deformed fluids. It also allows the characterization of wave properties and the flow pressure on structures.

The potential of SPH in simulating the interaction between waves and structures in coastal engineering was demonstrated by Nakao et al. [28], Wong [29], Kerényi et al. [30], and Zhu et al. [22]. They showed the SPH's effectiveness in accurately quantifying storm and tsunami wave characteristics. Positive results were obtained from investigations on the influence of these waves on both vertical and horizontal surfaces of nearshore structures, such as slab and girder bridges. Wei et al. [31] created an SPH model to study the interaction of a tsunami with a single bore, which had different diameters of 120 mm and 140 mm. The study investigated how various pile configurations affect the evolution of flow with free surfaces and the hydrodynamic load. Comparisons were made between the experimental measurements and transient flow velocities surrounding the bore. 3-D SPH and FE models with 600,000 particles were conducted by Pringana et al. [32] to predict the collision of a tsunami with a column situated on a dry bed.

2. SPH Method Overview

2.1. Principle

Based on the Lagrangian approach, the SPH method is mesh-free, and models flow by representing the system with discrete particles. The particles carry physical properties such as mass, density, and velocity, and the system evolves through interactions of particles under an external force. This is achieved through a specific integration process, represented by Equation 1:

$$f(r) = \int_{\Omega} f(r')W(r - r', h)dr' \quad (1)$$

in which f = continuous function of the position vector r , Ω = domain that includes the position vector r , W = smoothing kernel function, and h = smoothing length.

In this method, physical quantities at any point are calculated through a smoothing kernel function, which defines the influence area of each particle [17, 18] (see Figure 1). The particle interactions are governed by key equations such as the continuity equation for mass conservation, momentum equation for fluid motion [33, 34], and equation of state

for pressure-density relationships. The explicit Newmark integration scheme is used for time discretization [35], with appropriate time steps ensuring stability based on the Courant-Friedrichs-Lewy condition [36].

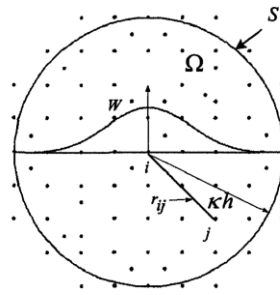


Figure 1. Support domain of W for particle i [25]

2.2. Boundary Conditions

Ghost particles are coupled with the Dynamic Boundary Condition Method (DBCM) for numerical simulations (Figure 2). Ghost particles are utilized for boundaries on the side walls and bottom of the channel, while DBCM is applied to handle the boundary conditions around complex bridge piers. This approach is effective in saving significant computational time with DBCM for large numbers of particles associated with the tank's bottom and side walls, while still preventing fluid particles from penetrating the boundaries of the complex bridge superstructure.

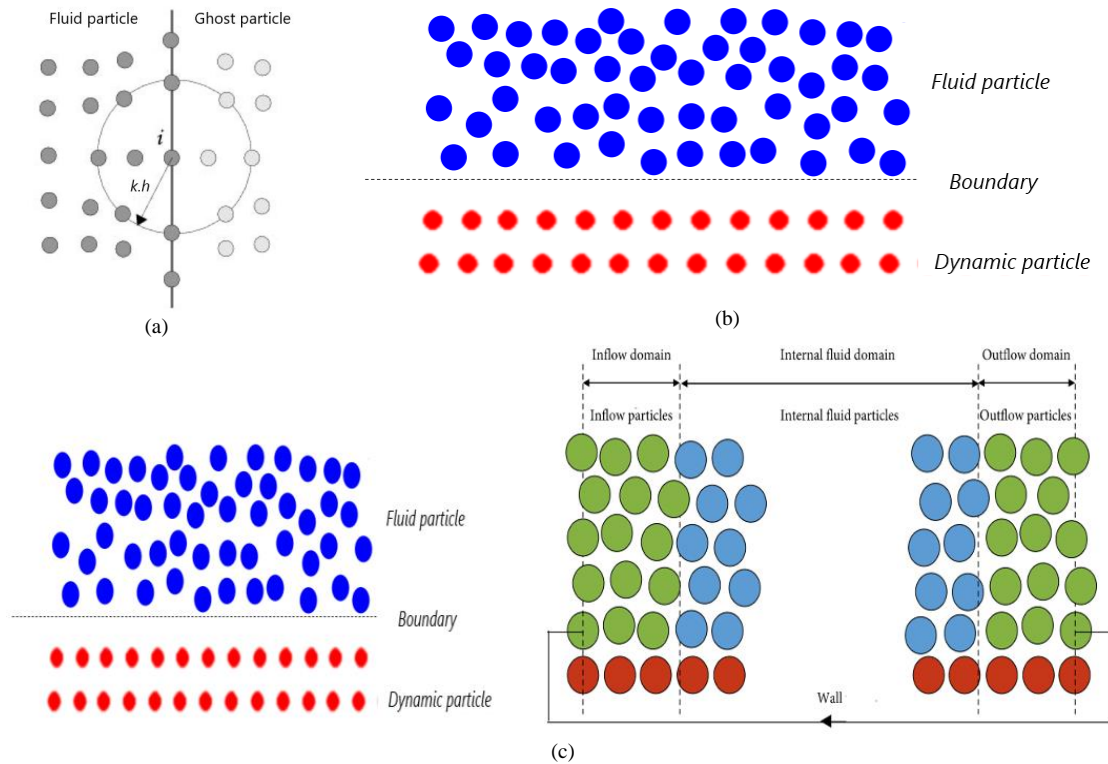


Figure 2. Boundary condition for fluid and solids: a) Ghost particle method; b) DBCM; c) Inflow-outflow boundary conditions in SPH simulation

Additionally, challenges arise in SPH simulations when dealing with inflow and outflow boundaries. Beyond setting the correct boundary conditions, managing particles that leave or enter the domain is crucial. To address this, inflow-outflow boundary conditions are implemented. This method assigns pressure conditions directly to inlet and outlet boundaries and uses homogeneous conditions for velocity. By treating both inlet and outlet boundaries similarly, the procedure effectively handles open boundaries with both positive (inflow) and negative (outflow) normal velocities.

2.3. Procedure of the Proposed SPH Simulation

The schematic diagram illustrating the SPH simulation for fluid-structure interaction in this study is proposed in Figure 3. The detailed steps are as follows:

- **Initialization:** The 2D simulation, coded and executed in MATLAB, starts with a total simulation time of 30 seconds and an initial particle spacing of $\Delta x = 20$ mm. The simulation domain is also defined.
- **Solid Boundary Treatment:** Boundary conditions are set for the perimeter of the T-beam superstructure and the riverbed.
- **Inlet/Outlet Boundary Treatment:** Boundary conditions for the inflow domain particles are set, defining the velocity, position, density, and pressure of each particle.
- **Nearest Neighbor Particle Search:** The neighbor particle search algorithm identifies particles within a radius h ($h = 2\Delta x$).
- **Kernel Function Calculation:** The kernel function value is computed for each particle.
- **Density Change Calculation:** The fluid density change is determined for each particle.
- **Energy and Momentum Change:** Velocity changes for each particle are computed.
- **Position, Velocity, Energy, and Density Update:** Particle velocity and position are updated over time.
- **Time Integration:** The time step is set to $\Delta t = 10^{-5}$ seconds.
- **Output:** The results are processed and presented after the simulation ends.

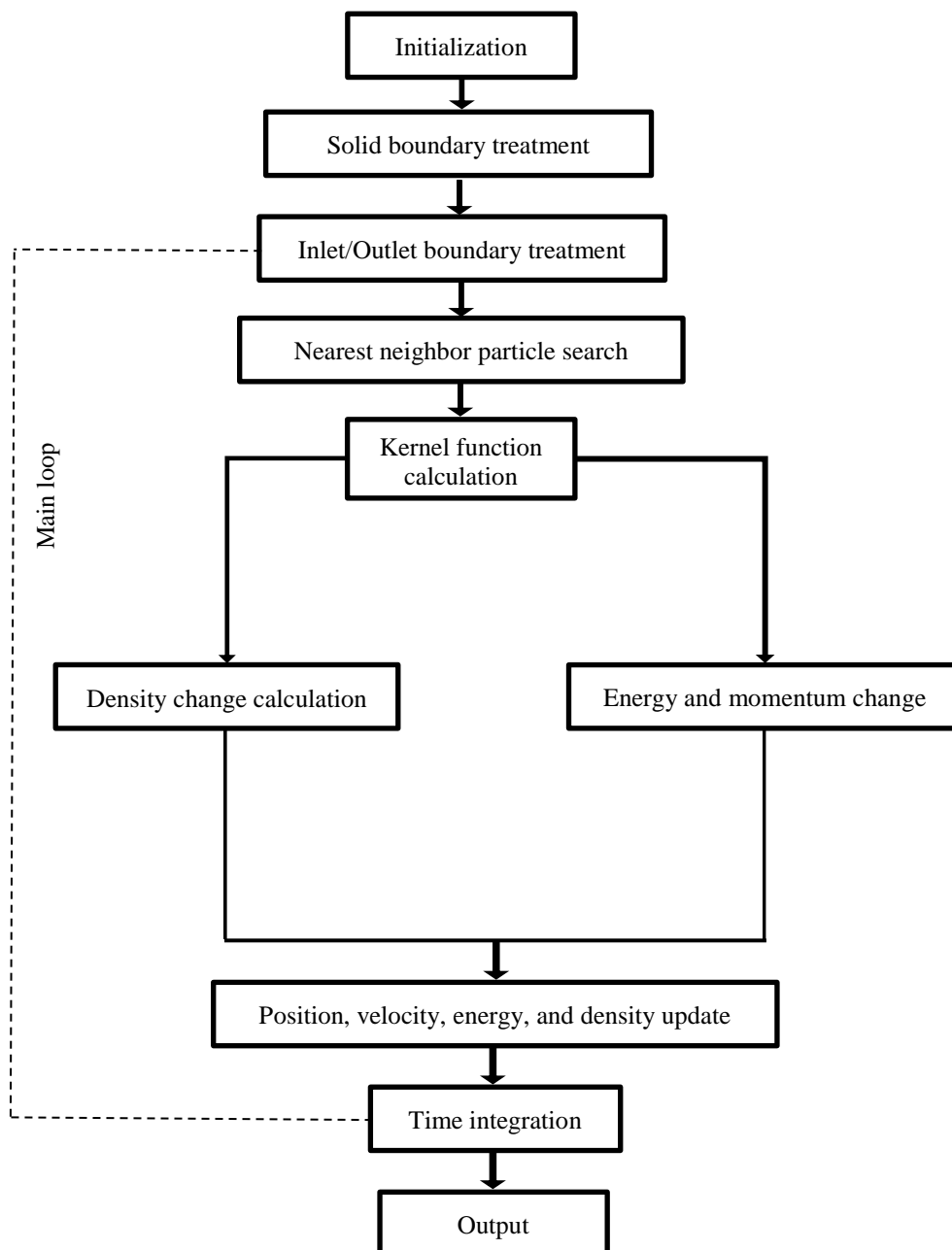


Figure 3. Flowchart of the SPH simulation for fluid-structure interaction in this study

3. A case study

3.1. Description of the Geometry of the SPH Model

In this section, a 2D SPH model is created to analyze flow pressure on the superstructure of Canh Nang bridge (located in Thanh Hoa province, Vietnam), which was damaged by a severe flood flow. The model is performed for the mid-span section, which corresponds to the deepest river-bed location (Figure 4). The distance from the bottom of the girders to the river-bed ground was measured to be 12.8 m. During the flood, the superstructure was submerged in the flood flow, and the maximum water level was observed to be 2.0 m below the bridge deck surface, and the water flowed at an average speed of $V = 2.5$ m/s. Other input parameters were measured as shown in Table 1. The 2D SPH model is utilized with the calculation domain configuration shown in Figure 5. Distances of 35 m in front of and 20 m behind the superstructure location are selected to ensure stability of the fluid flow in the numerical computation.

Table 1. Input parameters for Canh Nang bridge

Quantity	Notation	Value	Unit	Note
Flow direction relative to bridge centerline direction	θ	90	degree	
Average velocity of flood flow component in the direction of the stream centerline	V_x	2.5	m/s	
Velocity of flood flow component in the direction perpendicular to the stream centerline	V_{xc}	0	m/s	
Distance from the bottom of the girders to top of the guardrail ledge	d_{ss}	2.4	m	
Distance from the bottom of the girders to the top of the handrail	d_{sp}	2.8	m	
Distance from the bottom of the girders to the river-bed ground	y_{gs}	12.8	m	Average
Distance from the bottom of the girders to the top of the flood flow	d_{wgs}	4.4	m	



Figure 4. Canh Nang bridge (located in Thanh Hoa province, Vietnam) damaged by flood flow

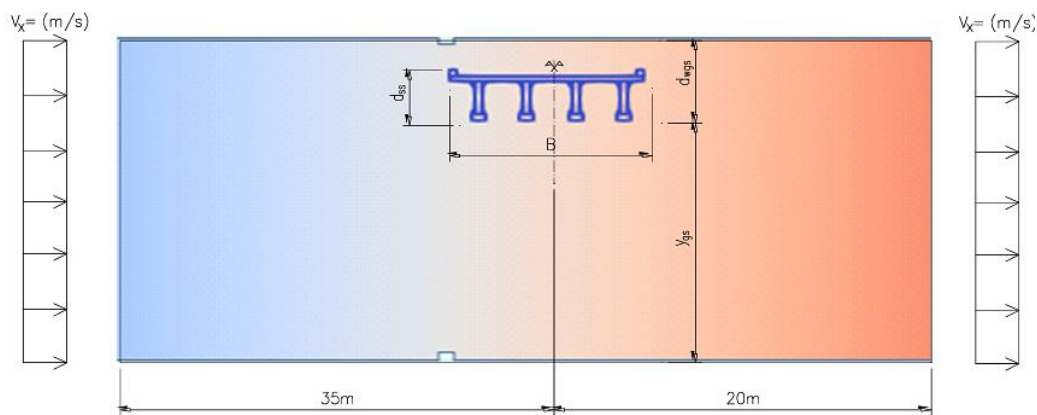


Figure 5. Domain of the SPH simulation

The outputs include time histories of flow pressure recorded by numerical probes. These pressure values are utilized to determine the forces exerted on the bridge. At a specific point on the bridge pier face, the force F_i can be calculated by Equation 2:

$$F = \sum F_i = \sum_1^n P_i A_i \tag{2}$$

where P_i is the pressure and A_i is the area at the probe i (Figure 6).

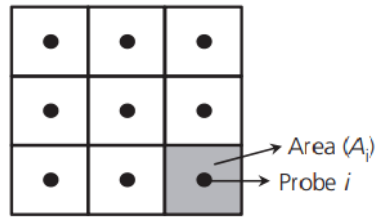
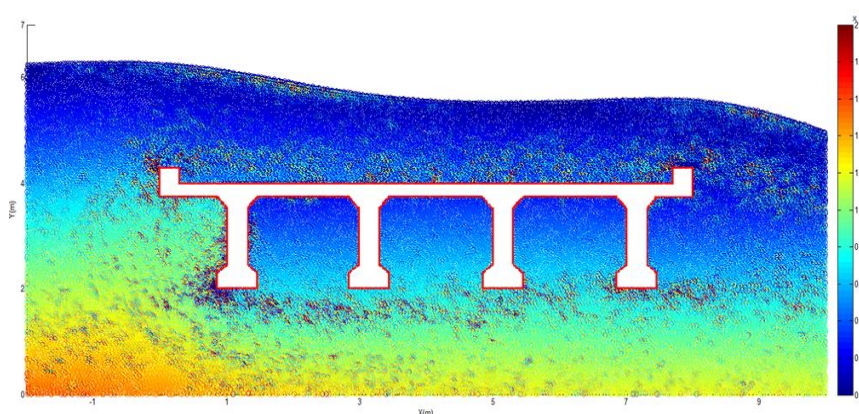
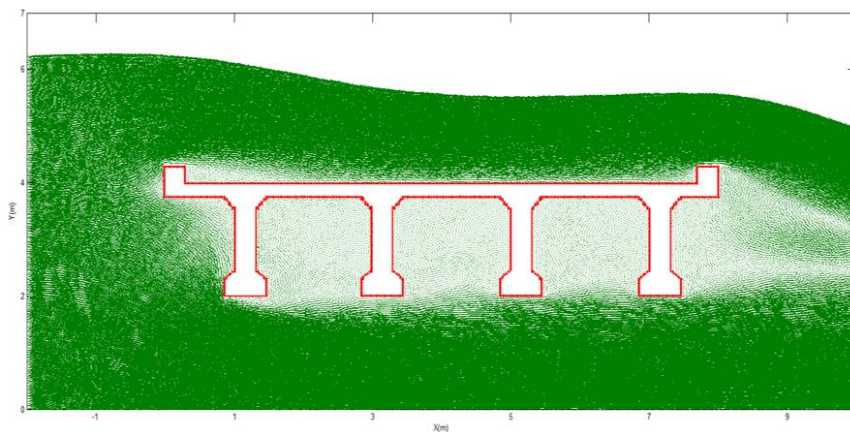


Figure 6. Probe arrangement on the structure's surface

3.2. Results and Discussion

The 2D calculation code using the SPH method is developed in the MATLAB programming language. The beam cross-section employs solid boundary condition elements along with elements representing the river bottom, which are assigned conditions assuming no change in position during the calculation. The distance between elements is selected as $dp = 2\text{cm}$, based on a study aimed at ensuring the accuracy of calculation results through a mesh convergence analysis. The minimum distance between particles is chosen to reduce volume and calculation time while still ensuring result accuracy. The distance dp of 2cm corresponds to an element count of approximately 600,000 for the liquid elements and approximately 50,000 for boundary condition elements. The calculation process takes place over 30 seconds with a calculation time step of $\Delta t = 10^{-5}$ s, in order to consider the period from which the flow begins to impact on the superstructure until the calculated value (flow pressure) stabilizes.

Calculation results from the SPH model include simulations of flow morphology, velocity fields, and flow pressure fields at all points of the structure around the flow. The calculation of flow pressure on the structure is performed at any location on the girder surface. Based on the horizontal pressure of the flow, the horizontal thrust of the flow on the superstructure can be calculated. Figure 7 shows the velocity and flow pressure fields during flow impact simulations at several times: $t = 10$ s, 20 s, and 30 s. The results indicate that the flow pressure reaches its highest value on the girder surface at positions adjacent to the guardrail ledge and the exterior girder bulb. This occurs because these areas create local water flow resistance, leading to a sudden change in flow direction (refer to Figure 8). In contrast, water in the areas between the two girders exhibits low circulation speeds, resulting in local vortex regions. Meanwhile, the flow beneath the girder bottom elevation circulates vigorously, with a velocity close to the water flow's average velocity.



(a) $t = 10$ s

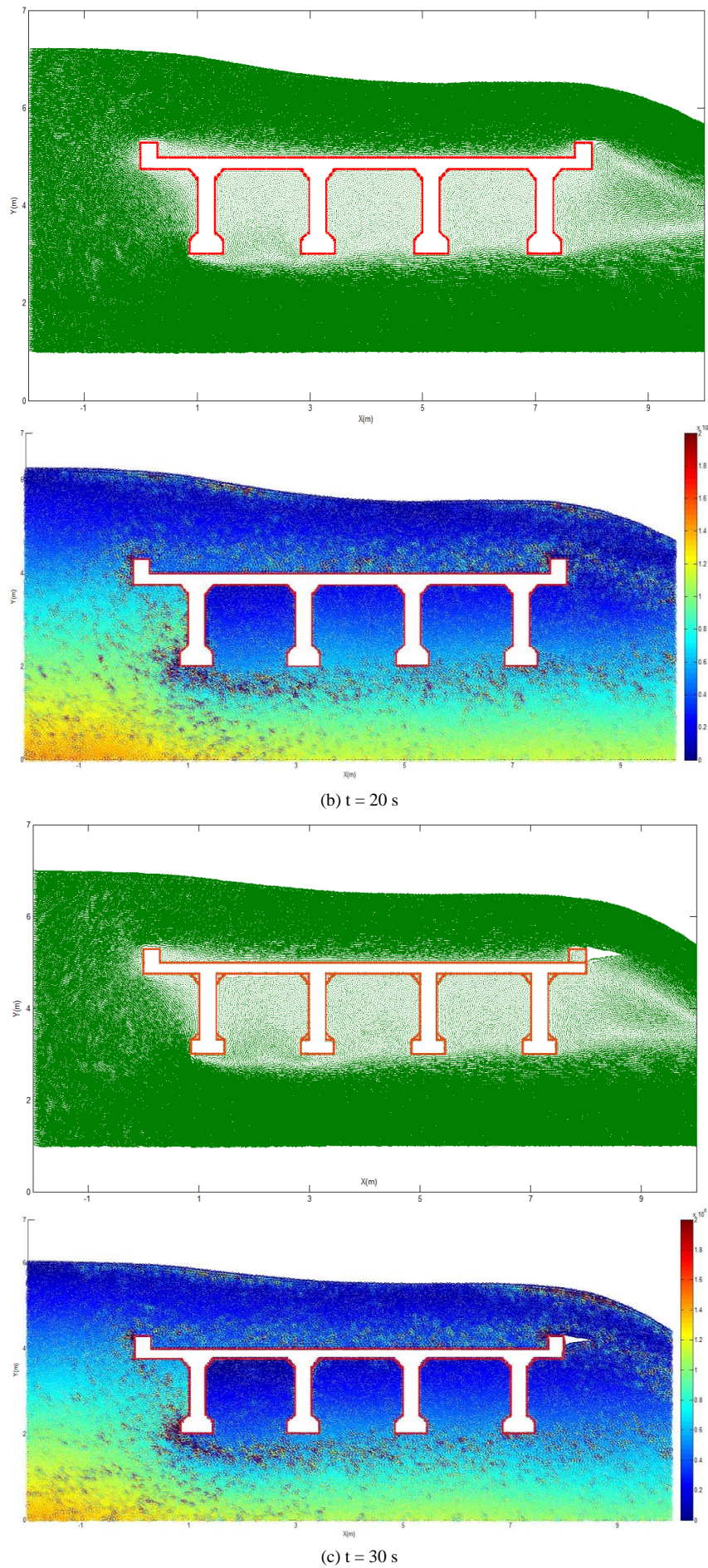


Figure 7. Snapshots taken at different times of a flow impacting the superstructure

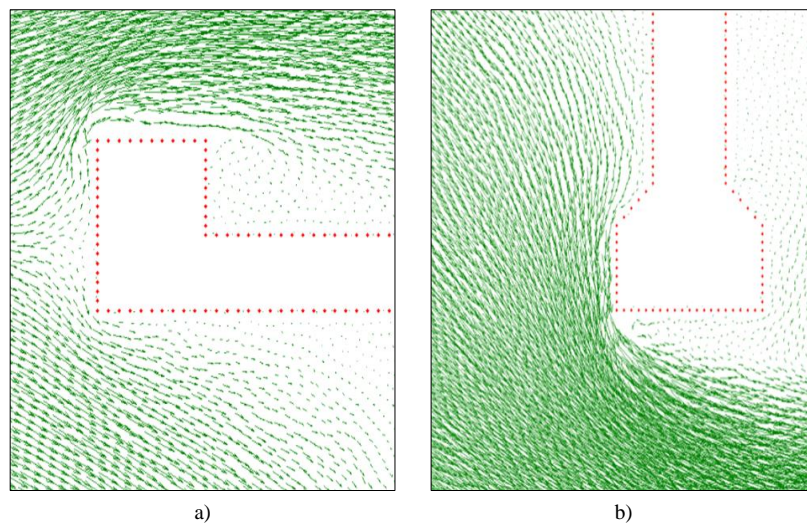


Figure 8. Locations subjected to high flow pressure at a) the guardrail ledge, and b) bottom of the exterior girder

Figure 9 shows the calculated values of the horizontal pressure of the flow at several representative points on the surface of the girders. The calculation time is carried out over 30 seconds, which is sufficient for the flow to remain stable. To analyze the calculated results, several key points around the cross-section of the girders are selected: the midpoint of the water-facing side of the guardrail (Pt), the midpoint of the water-facing side of the girder webs (Ps1–Ps4), and the midpoint of the water-facing side of the girder bottoms (Pb1–Pb4). In the initial stage, when the flow begins to move and collide with the superstructure, the pressure of the flow peaks at the highest value at all the points of interest (Pt, Ps1, Pb1, Ps2, Pb2, Ps3, Pb3, Ps4, and Pb4). The peak value is 25% greater than that of the flow in the stable phase afterward and then is gradually decreasing.

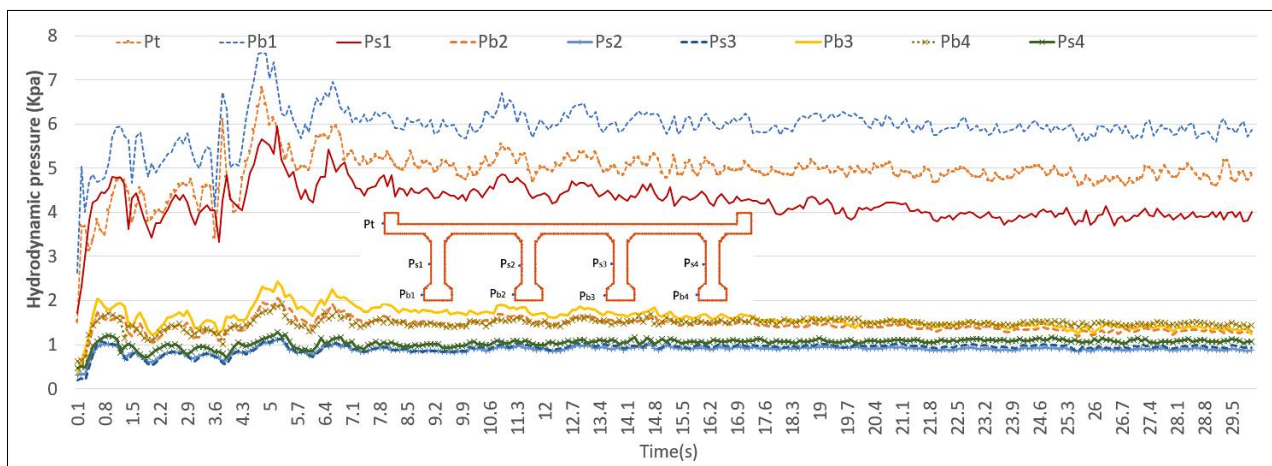


Figure 9. Horizontal pressure of the flow on the surfaces of the girders computed by the SPH model

In the stable phase (after 20 s), the flow pressure varies throughout the different points of interest, in which the highest value is observed at the midpoint of the exterior girder's bulb (Pb1), followed by that at the top of the guardrail ledge (Pt) and the midpoint of the exterior girder's web (Ps1). The average flow pressure values at these points are 5.82, 4.79, and 3.86 kPa, respectively.

The average flow pressure values on the interior girders' bulbs at Points Pb2, Pb3, and Pb4 are 1.31, 1.44, and 1.50 kPa, respectively. The average flow pressure values on the interior girders' webs at Points Ps2, Ps3, and Ps4 are 0.82, 0.92, and 1.15 kPa, respectively. The results show a large difference in the flow pressure values at the points of interest: the pressure at the interior girders' surfaces is approximately 14%-25% lower than that at the exterior girder's surface, which is in direct contact with the water flow. This difference is due to the formation of a "water blockage" zone between the girders, where the water flow velocity is low, moving only in local vortices between adjacent girders, thus reducing the horizontal pressure of the water flow. The "water blockage" zone is clearly shown in Figure 7, which presents the flow velocity field. Between the interior girders, vortices form as water particles move in circular patterns, revealing local flow velocity and morphology that cannot be captured by CFD or VOF methods.

The SPH flow pressure values for Canh Nang bridge are also compared with those calculated according to bridge design standards, including AS5100 [37], Eurocode (B. 59/94.) [38], TCVN 11823 [39], and Indian Code [40], as shown in Figure 10. The value calculated at the exterior girder's side by the proposed SPH model is greater than those computed

based on the bridge design codes. Specifically, the maximum pressure value at Pb1 is 125.04%, 110.84%, 169.42%, and 159.33% higher than those calculated according to the AS5100, BA 59/94, TCVN 11823, and Indian codes, respectively. The maximum pressure value at Pt compared to those computed based on the AS5100, BA 59/94, TCVN 11823, and Indian codes is 111.75%, 99.05%, 151.42%, and 142.39%, respectively. Similarly, the maximum pressure value at Ps1 compared to those computed based on the AS5100, BA 59/94, TCVN 11823, and Indian codes is 97.64%, 86.54%, 132.59%, and 124.41%, respectively.

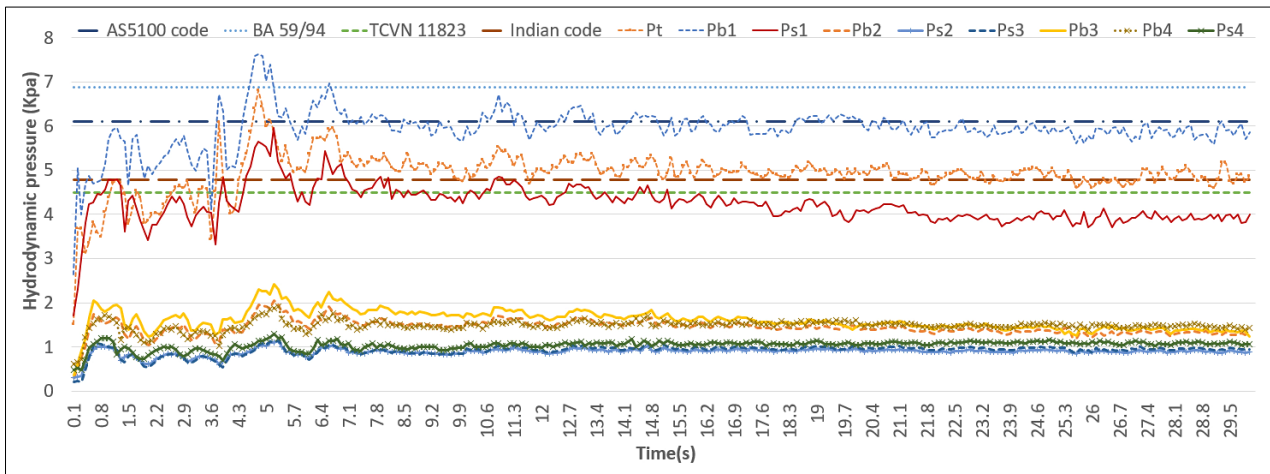


Figure 10. Horizontal flow pressure on girders' surfaces according to different calculation methods

The pressure values on the interior girders are significantly smaller than those on the exterior girder. These SPH pressure values are also lower than those computed using the other codes. Especially, the maximum pressure value at Pb3 (Girder #3) compared to those computed according to the AS5100, BA 59/94, TCVN 11823, and Indian codes is 39.72%, 35.20%, 53.81%, and 50.60%, respectively.

Overall, when comparing the SPH model results with the current standards AS5100, BA 59/94, TCVN 11823, and Indian codes, the flow pressure values calculated according to these bridge design standards exhibit common characteristics. These values depend on the flow velocity (V), the wetted area of the superstructure (A), and the water resistance coefficient (C_d), which varies based on the shape of the bridge structure. It is important to note that the flow velocity in these design codes is considered the average flow value. Consequently, the current bridge design standards do not account for localized pressure values at each point on the superstructure's surface. They fail to evaluate the effect of the "water blockage" phenomenon between the girders and do not consider the dynamic pressure effect of the flow on the structure during the initial stage when the flow contacts and collides with the exterior girders. This limitation is a notable drawback of the current bridge design standards.

4. Analysis of Flow Condition Parameters Affecting the Water Resistance Coefficient of the Superstructure

The proposed SPH model is then used to analyze parameters affecting the flow pressure on the superstructure. In order to represent the interaction between the flow and the superstructure, the water resistance coefficient of the superstructure (C_d) is used. Among the current bridge design codes mentioned above, only the AS5100 code takes into account the influence of flow-related parameters on the coefficient C_d , while in the other codes, C_d only depends on the structure's shape or simply is a constant value.

The parameters influencing the coefficient C_d in the AS5100 code are the submergence parameter (S_r) and the position parameter (P_r) (see Figure 11) calculated using the following relationships.

$$S_r = \frac{dwgs}{dss} \tag{3}$$

$$P_r = \frac{ysg}{dss} \tag{4}$$

The submergence coefficient $S_r = 1.83$ corresponds to the case study of Canh Nang Bridge. The position parameter $P_r = 5.625$ is used in comparison cases (S_r varies from 0.5 to 3.5). According to AS5100, the value of C_d varies from 1.39 to 1.95 when S_r changes from 0.5 to 3.5. In other standards, a constant value of C_d is taken that is independent of S_r . The calculation results of the influence of the submergence coefficient S_r on the water resistance coefficient C_d are also compared with the study results of Guo et al. [41] as shown in Figure 12. When S_r increases from 1 to 3.5, there is a similarity in the C_d value trends computed by the three methods: AS5100, SPH, and Guo et al. [41]. Remarkably, the SPH model results agree well with those of Guo et al. [41] for the S_r range of 2.5 and 3.5.

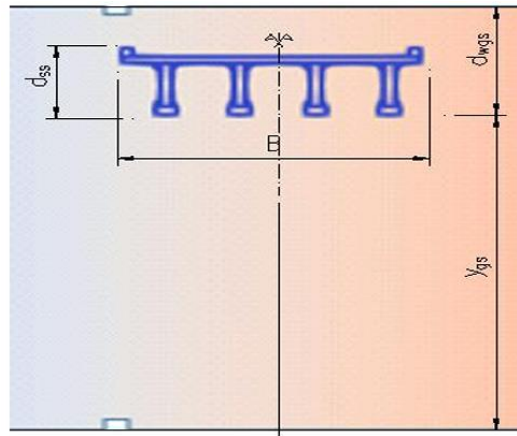


Figure 11. Parameters affecting the flow pressure on the submerged structure

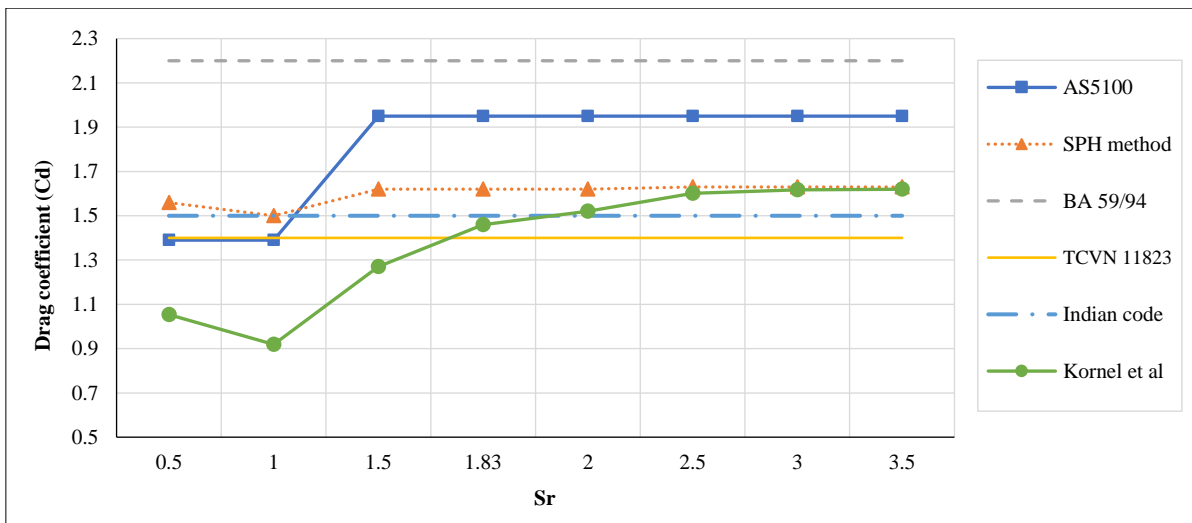


Figure 12. Effect of submergence coefficient (Sr) on water resistance coefficient (Cd) of superstructure

The influence of the superstructure position coefficient (Pr) on the flow pressure is also investigated using the SPH model, in which Pr varies from 1.5 to 8.0 while Sr remains constant at 1.833. According to the AS5100 code, Cd largely varies from 3.35 to 1.8 when Pr changes from 1.5 to 8.0; however, the Cd value computed by the SPH model slightly varies from 2.1 to 1.57. The influence of Pr on Cd is shown in Figure 13. The Cd values calculated according to other design standards are constants, in which the Eurocode provides the highest value while the TCVN 11823 yields the lowest value. It should be noted that the Cd values computed based on the AS5100 code are the high values when considering both Sr and Pr parameters.

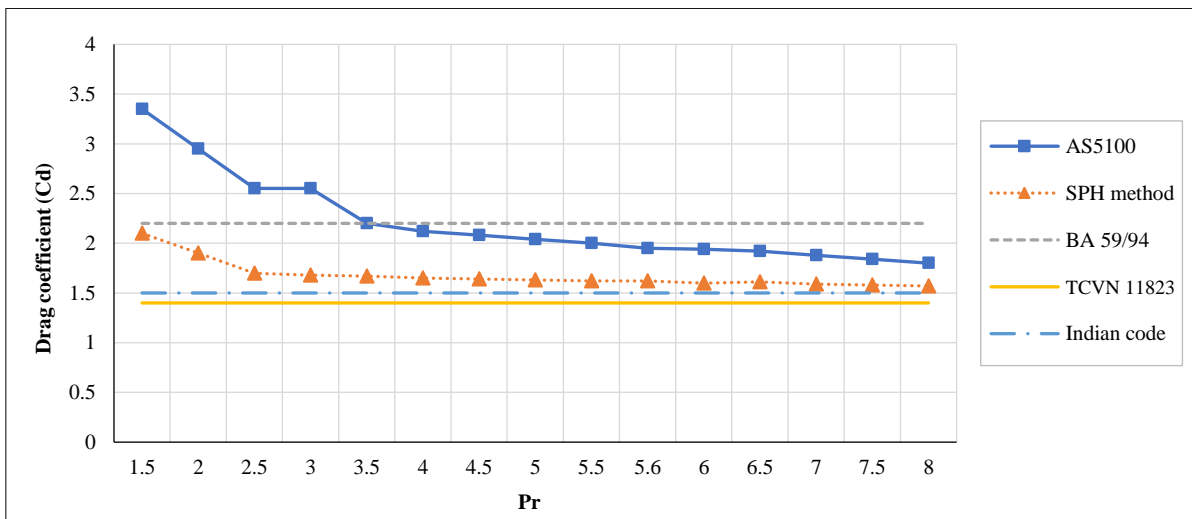


Figure 13. Effect of position coefficient (Pr) on the water resistance coefficient (Cd) of superstructure

5. Conclusion

In this study, a numerical simulation using the SPH method was developed to model the impact of water flow on the superstructure of a bridge. The simulation involved 600,000 fluid elements and 50,000 boundary condition elements over a 30-second computation period, with a fixed time step of 10^{-5} s. Modified dynamic boundary conditions for solid surfaces and inflow-outflow boundaries were incorporated to effectively handle interactions between fluid and beds, and fluid and structures. The SPH model was applied to the Canh Nang bridge in Vietnam, which was damaged by severe flooding. Geometric dimensions and flow characteristics were measured onsite, enabling the simulation to capture flow morphology, velocity fields, and flow pressure around the submerged superstructure. The results revealed that high flow pressure occurred on direct surfaces of the superstructure, while lower pressure was observed on the bottom surfaces and between adjacent girders. The water resistance coefficient (C_d) was also calculated based on these pressure values.

Additionally, comparisons of the SPH model results were made with those calculated using other bridge design standards, such as the Indian code, Eurocode, AS5100, and TCVN 11823. The SPH model demonstrated advantages in capturing flow dynamics in such scenarios. Future studies should focus on experimental validation to enhance the accuracy of the SPH model. Moreover, further research is necessary to examine the influence of structural parameters, such as the shape and size of the bridge's superstructure, on its response to flow impact during flood events.

6. Declarations

6.1. Author Contributions

Conceptualization, T.A.D. and T.H.N.; methodology, T.A.D. and T.H.N.; software, T.H.N.; validation, T.A.D.; investigation, T.H.N.; data curation, T.H.N.; writing—original draft preparation, T.A.D. and T.H.N.; writing—review and editing, T.A.D. All authors have read and agreed to the published version of the manuscript.

6.2. Data Availability Statement

The data presented in this study are available in the article.

6.3. Funding

This study is funded by Vietnam Ministry of Education and Training under the grant number B2023-GHA-04.

6.4. Conflicts of Interest

The authors declare no conflict of interest.

7. References

- [1] Cao, M. X., Liu, Z., & Meng, J. (2009). Statistical analysis and reflections on bridge deficiencies and disasters in the United States. *Highway*, 7(7), 162-167.
- [2] Storey, C., & Delatte, N. (2003). Lessons from the Collapse of the Schoharie Creek Bridge. *Forensic Engineering* (2003), 158–167. doi:10.1061/40692(241)18.
- [3] Sousa, J. J., & Bastos, L. (2013). Multi-temporal SAR interferometry reveals acceleration of bridge sinking before collapse. *Natural Hazards and Earth System Science*, 13(3), 659–667. doi:10.5194/nhess-13-659-2013.
- [4] Saatcioglu, M., Ghobarah, A., & Nistor, I. (2006). Performance of structures in Thailand during the December 2004 Great Sumatra earthquake and Indian Ocean tsunami. *Earthquake Spectra*, 22(SUPPL. 3), 295–319. doi:10.1193/1.2209175.
- [5] Kawashima, K., Kosa, K., Takahashi, Y., Akiyama, M., Nishioka, T., Watanabe, G., ... & Matsuzaki, H. (2011). Damages of bridges during 2011 Great East Japan earthquake. *Proceedings of 43rd Joint Meeting, US-Japan Panel on Wind and Seismic Effects*, 29-30 August, Tsukuba Science City, Japan.
- [6] Hirt, C. W., & Nichols, B. D. (1981). Volume of fluid (VOF) method for the dynamics of free boundaries. *Journal of Computational Physics*, 39(1), 201–225. doi:10.1016/0021-9991(81)90145-5.
- [7] Xiao, H., Huang, W., Tao, J., & Liu, C. (2013). Numerical modeling of wave-current forces acting on horizontal cylinder of marine structures by VOF method. *Ocean Engineering*, 67, 58–67. doi:10.1016/j.oceaneng.2013.01.027.
- [8] Nan, X., Liu, X., Chen, L., Yan, Q., & Li, J. (2023). Study of the bridge damage during flooding based on a coupled VOF-FSI method. *Journal of Engineering Research (Kuwait)*, 11(3), 51–61. doi:10.1016/j.jer.2023.100081.
- [9] Song, Y., Jia, J., Liu, H., Chen, F., & Fang, Q. (2023). Numerical Study on Tsunami Force on Coastal Bridge Decks with Super-elevation. *Journal of Marine Science and Engineering*, 11(4), 824. doi:10.3390/jmse11040824.

- [10] Tang, C., Zhao, Q., Wang, L., Chen, Z., & Fang, Q. (2024). Numerical Investigation of Wave Force on Coastal Bridge Decks Close to a Sloping Seabed. *Journal of Marine Science and Engineering*, 12(6), 984. doi:10.3390/jmse12060984.
- [11] Han, W., Xu, X., Wang, J., Xiao, L., Zhou, K., & Guo, X. (2023). Safety Assessment of Coastal Bridge Superstructures with Box Girders under Potential Landslide Tsunamis. *Journal of Marine Science and Engineering*, 11(5). doi:10.3390/jmse11051062.
- [12] Wang, S., Liu, S., Xiang, C., Li, M., Yang, Z., & Huang, B. (2023). Prediction of Wave Forces on the Box-Girder Superstructure of the Offshore Bridge with the Influence of Floating Breakwater. *Journal of Marine Science and Engineering*, 11(7), 1326. doi:10.3390/jmse11071326.
- [13] Kisi, O., Ardiçlioğlu, M., Hadi, A. M. W., Kuriqi, A., & Kulls, C. (2023). Estimation of Mean Velocity Upstream and Downstream of a Bridge Model Using Metaheuristic Regression Methods. *Water Resources Management*, 37(14), 5559–5580. doi:10.1007/s11269-023-03618-6.
- [14] Kosa, K., Akiyosi, S., Nii, S., & Kimura, K. (2017). Experimental study to evaluate the horizontal force to the bridge by tsunami, *Kozo Kogaku Ronbunshu. Journal of Structural Engineering*, 57.
- [15] Liang, T., Ohmachi, T., Inoue, S., & Lukkunaprasit, P. (2011). Experimental and Numerical Modeling of Tsunami Force on Bridge Decks. In *Tsunami - A Growing Disaster* (pp. 105–130). doi:10.5772/23622.
- [16] Zhang, G., Usui, T., & Hoshikuma, J. (2010). Experimental Study on a Countermeasure for Reducing Tsunami Wave Force Acting on Superstructure of Bridges. *Journal of Japan Society of Civil Engineers, Ser. A1 (Structural Engineering & Earthquake Engineering (SE/EE))*, 66(1), 425–433. doi:10.2208/jscejsee.66.425.
- [17] Gingold, R. A., & Monaghan, J. J. (1977). Smoothed particle hydrodynamics: theory and application to non-spherical stars. *Monthly Notices of the Royal Astronomical Society*, 181(3), 375–389. doi:10.1093/mnras/181.3.375.
- [18] Lucy, L. B. (1977). A numerical approach to the testing of the fission hypothesis. *The Astronomical Journal*, 82, 1013. doi:10.1086/112164.
- [19] Nguyen, Q. B. (2009). Reliability of industrial installations under impact of structural fragments - Domino effect. Ph.D. Thesis, Paris, France. (In French).
- [20] Xu, F., Zhao, Y., Yan, R., & Furukawa, T. (2013). Multidimensional discontinuous SPH method and its application to metal penetration analysis. *International Journal for Numerical Methods in Engineering*, 93(11), 1125–1146. doi:10.1002/nme.4414.
- [21] Shintate, K., & Sekine, H. (2004). Numerical simulation of hypervelocity impacts of a projectile on laminated composite plate targets by means of improved SPH method. *Composites Part A: Applied Science and Manufacturing*, 35(6), 683–692. doi:10.1016/j.compositesa.2004.02.011.
- [22] Zhu, M., Elkhetafi, I., & Scott, M. H. (2018). Validation of OpenSees for Tsunami Loading on Bridge Superstructures. *Journal of Bridge Engineering*, 23(4), 4018015. doi:10.1061/(asce)be.1943-5592.0001221.
- [23] Do, T. A., Nguyen, T. H., Nguyen, H. M., Tran, N. D., & Nguyen, L. N. (2020). Evaluation of dynamic impact of flow with bridge pier using smoothed particle hydrodynamics method. *Progress in Computational Fluid Dynamics*, 20(6), 332–348. doi:10.1504/PCFD.2020.111401.
- [24] Nguyen-Ngoc, L., Do, T. A., Nguyen, T. H., Nguyen, T. D., Tran, A. T., Ho, N. X., & Nguyen, D. H. (2023). Smoothed Particle Hydrodynamics Simulation and Evaluation of Water Flow Pressure on Bridge Piers. *Journal of Applied Science and Engineering*, 26(10), 1471–1479. doi:10.6180/jase.202310_26(10).0012.
- [25] Nguyen, H. T., Cosson, B., Lacrampe, M. F., & Do, T. A. (2018). Numerical simulation of reactive polymer flow during rotational molding using smoothed particle hydrodynamics method and experimental verification. *International Journal of Material Forming*, 11(4), 583–592. doi:10.1007/s12289-017-1367-2.
- [26] Nguyen, H. T., Do, T. A., & Cosson, B. (2019). Numerical simulation of submerged flow bridge scour under dam-break flow using multi-phase SPH method. *Mathematical Biosciences and Engineering*, 16(5), 5395–5418. doi:10.3934/mbe.2019269.
- [27] Shao, S., & Lo, E. Y. M. (2003). Incompressible SPH method for simulating Newtonian and non-Newtonian flows with a free surface. *Advances in Water Resources*, 26(7), 787–800. doi:10.1016/S0309-1708(03)00030-7.
- [28] Nakao, H., Zhang, G., Sumimura, T., & Hoshikuma, J. I. (2013). Numerical assessment of tsunami-induced effect on bridge behavior. *Proceedings of the 29th US-Japan Bridge Engineering Workshop*, 11-13, November, Tsukuba, Japan.
- [29] Wong, H. K. (2015). Three-dimensional effects of tsunami impact on bridges. Master Thesis, University of Washington, Seattle, United States.
- [30] Kerenyi, K., Sofu, T., & Guo, J. (2009). Hydrodynamic forces on inundated bridge decks. FHWA-HRT-09-028, United States Department of Transportation, McLean, United States.

- [31] Wei, Z., Dalrymple, R. A., Hérault, A., Bilotta, G., Rustico, E., & Yeh, H. (2015). SPH modeling of dynamic impact of tsunami bore on bridge piers. *Coastal Engineering*, 104, 26–42. doi:10.1016/j.coastaleng.2015.06.008.
- [32] Pringgana, G., Cunningham, L. S., & Rogers, B. D. (2016). Modelling of tsunami-induced bore and structure interaction. *Proceedings of the Institution of Civil Engineers: Engineering and Computational Mechanics*, 169(3), 109–125. doi:10.1680/jenm.15.00020.
- [33] Dalrymple, R. A., & Rogers, B. D. (2006). Numerical modeling of water waves with the SPH method. *Coastal Engineering*, 53(2–3), 141–147. doi:10.1016/j.coastaleng.2005.10.004.
- [34] Gotoh, H., Shao, S., & Memita, T. (2004). SPH-LES model for numerical investigation of wave interaction with partially immersed breakwater. *Coastal Engineering Journal*, 46(1), 39–63. doi:10.1142/S0578563404000872.
- [35] Ata, R., & Soulaïmani, A. (2005). A stabilized SPH method for inviscid shallow water flows. *International Journal for Numerical Methods in Fluids*, 47(2), 139–159. doi:10.1002/flid.801.
- [36] Courant, R., Friedrichs, K., & Lewy, H. (1928). On the partial difference equations of mathematical physics. *Mathematische Annalen*, 100(1), 32–74. doi:10.1007/BF01448839.
- [37] AS 5100.1-2004 AP-G15.1/04. (2004). *Bridge Design, Part 1: Scope and General Principles*. Australian Standard, Sydney, Australia.
- [38] B. 59/94. (1994). *Design of highway bridges for hydraulic action (Part 6)*. The Scottish Office development Department, The Welsh office, The Department of the Environment for Northern Ireland, Belfast, Northern Ireland.
- [39] TCVN11823:2017. (2017). *Highway bridge design specification*. Vietnam Standards, Hanoi, Vietnam. (In Vietnamese).
- [40] IRC:58-2015. (2015). *Guidelines for the Design of Plain Jointed Rigid Pavements for Highway (4th Ed.)*. Indian Roads Congress, New Delhi, India.
- [41] Guo, J., Kerenyi, K., Pagan-Ortiz, J. E., Flora, K., Lyn, D., & Bergendahl, B. (2009). *Bridge Pressure Flow Scour for Clear Water Conditions*. FHWA-HRT-09-041, United States Department of Transportation, McLean, United States.